Physica D 55 (1992) 328-339

Third Generation Cellular Automaton for Modeling Excitable Media*

Jörg R. Weimar †

John J. Tyson ‡

Layne T. Watson†

Abstract. This paper introduces a new cellular automaton model of excitable media with improved treatments of (1) diffusion and wave propagation, and (2) slow dynamics of the recovery variable. The automaton is both computationally efficient and faithful to the underlying partial differential equations.

1. Introduction

Excitable media support undamped traveling waves of excitation, such as waves of oxidation in certain chemical reaction systems and waves of membrane depolarization in nerve axons. Some simple models, consisting of a pair of partial differential equations, have become popular representations of excitable media, e.g., the Oregonator model [3, 10,15] of the Belousov-Zhabotinskii reaction [20,22], and the FitzHugh-Nagumo model [1, 4] of neuromuscular membranes. But the earliest model (1946) of excitable media was a

* This work was supported in part by National Science Foundation Grant DMS-8810456 and Department of Energy Grant DE-FG05-88ER25068. A preliminary version of this paper was presented at the Fifth SIAM Conference on Parallel Processing for Scientific Computation.

† Department of Computer Science, Virginia Polytechnic Institute and State University, Blacksburg, Virginia 24061-0106, e-mail: weimar@cayuga.cs.vt.edu

‡ To whom correspondence should be addressed: Department of Biology, Virginia Polytechnic Institute and State University, Blacksburg, Virginia 24061-0406, e-mail: tyson@vtvm1.cc.vt.edu

discrete state model introduced by Wiener and Rosenblueth [19]. The cellular automaton approach was pursued first by Moe et al. [14], and later by Greenberg and Hastings [8, 9], and others. These "first generation models" featured nearest neighbor connections and only a few possible states per cell. Although they exhibited wave propagation, they failed in several crucial aspects [21]:

- The curvature effect: A wavefront that is curved backward should travel slower than a planar wave, which in turn should be slower than a wavefront that is curved forward. In particular, $N = c - D\,K$, where N is the normal velocity, K is the curvature, D is the diffusion coefficient of the excitation variable, and c is the planar wave speed.
- Dispersion relation: A wavefront can propagate not only into resting medium, but also into partially recovered medium. In this case the speed of the traveling wave should be slower than the speed of propagation into fully recovered (resting) medium.
- Spatial isotropy: The shape of spirals in these early models is always angular, not smooth, due to the nearest-neighbor-only connections and the resulting anisotropic speed of propagation.

These three shortcomings are addressed in "second generation" models by Gerhardt, Schuster and Tyson [5,6,7], Markus and Hess [12,13], and Efimov and Fast [2].

To model curvature effects, Gerhardt, Schuster and Tyson introduce bigger neighborhoods: squares of size $(2r+1)^2$, where $r = 1, \cdots, 6$. In their automaton the number of excited cells within this square neighborhood is counted and a resting cell becomes excited if this count exceeds a certain threshold. By making the threshold a linear function of the recovery state, they introduce dispersion into the automaton. Unfortunately, their automaton still exhibits some directional anisotropy.

Markus and Hess address the problem of directional anisotropy by introducing semi-random grids. They randomize the position of a grid point within its unit square, and then mark all neighbors within a circular boundary centered on the grid point. In this manner they achieve good spatial isotropy at the cost of high computational complexity.

Efimov and Fast recognize that for determining whether a cell should become excited, the excitation of a nearby cell has a bigger effect than the excitation of a cell that is far away. They calculate a weighted sum of excitation of cells in the neighborhood, where cells close to the center have high weights and cells far away have low weights. In general, the computation of such weighted sums is computationally expensive.

This paper introduces a "third generation" automaton that combines the strengths and avoids the weaknesses of these earlier versions. Furthermore, the cellular automaton (CA) rules are closely related to the underlying partial differential equations.

2. Description of new mask

Gerhardt, Schuster and Tyson favor a square mask because the operation of counting the number of excited neighbors can be done in a time independent of the size of the mask. This property is very desirable, especially for big masks. A square mask can be constructed as the convolution of a vertical strip and a horizontal strip. The sum within a strip is calculated by a scanning operation.

Another mask (a diamond mask) can be constructed as the convolution of two diagonal strips. The convolution of a square mask and a diamond mask generates a third mask, the one we prefer. Such "combination" masks are weighted more heavily in the center (e.g., Figure 1). Nonetheless, the results of its application to a data array can be calculated with 8 addition operations per cell, independent of the size of the mask. The example

$$\text{Mask} = \begin{bmatrix}
0 & 0 & 0 & 0 & 1 & 1 & 1 & 1 & 1 & 1 & 1 & 0 & 0 & 0 & 0 \\
0 & 0 & 0 & 1 & 2 & 3 & 3 & 3 & 3 & 3 & 2 & 1 & 0 & 0 & 0 \\
0 & 0 & 1 & 2 & 4 & 5 & 6 & 6 & 6 & 5 & 4 & 2 & 1 & 0 & 0 \\
0 & 1 & 2 & 4 & 6 & 8 & 9 & 10 & 9 & 8 & 6 & 4 & 2 & 1 & 0 \\
1 & 2 & 4 & 6 & 9 & 11 & 13 & 13 & 13 & 11 & 9 & 6 & 4 & 2 & 1 \\
1 & 3 & 5 & 8 & 11 & 14 & 16 & 17 & 16 & 14 & 11 & 8 & 5 & 3 & 1 \\
1 & 3 & 6 & 9 & 13 & 16 & 19 & 20 & 19 & 16 & 13 & 9 & 6 & 3 & 1 \\
1 & 3 & 6 & 10 & 13 & 17 & 20 & 21 & 20 & 17 & 13 & 10 & 6 & 3 & 1 \\
1 & 3 & 6 & 9 & 13 & 16 & 19 & 20 & 19 & 16 & 13 & 9 & 6 & 3 & 1 \\
1 & 3 & 5 & 8 & 11 & 14 & 16 & 17 & 16 & 14 & 11 & 8 & 5 & 3 & 1 \\
1 & 2 & 4 & 6 & 9 & 11 & 13 & 13 & 13 & 11 & 9 & 6 & 4 & 2 & 1 \\
0 & 1 & 2 & 4 & 6 & 8 & 9 & 10 & 9 & 8 & 6 & 4 & 2 & 1 & 0 \\
0 & 0 & 1 & 2 & 4 & 5 & 6 & 6 & 6 & 5 & 4 & 2 & 1 & 0 & 0 \\
0 & 0 & 0 & 1 & 2 & 3 & 3 & 3 & 3 & 3 & 2 & 1 & 0 & 0 & 0 \\
0 & 0 & 0 & 0 & 1 & 1 & 1 & 1 & 1 & 1 & 1 & 0 & 0 & 0 & 0
\end{bmatrix}$$

Figure 1: *Effective weights in the mask diamond(2)∗square(3).*

(Fig. 1) uses a square mask of radius 3 and a diamond mask that is constructed from diagonal strips of length 5 (radius 2). This mask, suitably normalized, is a good finite-difference approximation to the diffusion operator $\mathcal{D}_m \nabla^2$. Previously [18], we showed that the effective diffusion coefficient of the mask can be calculated from

$$\mathcal{D}_m = \frac{\sum_{m=0}^{\infty} \sum_{n=1}^{\infty} (m^2 + n^2) a_{m,n}}{a_{0,0} + 4 \sum_{m=0}^{\infty} \sum_{n=1}^{\infty} a_{m,n}}, \tag{1}$$

where $a_{m,n}$ are the elements of the mask (centered on $m = 0, n = 0$). For the mask in Figure 1, $\mathcal{D}_m = 4$.

When we use such masks to simulate wave propagation in excitable media, we desire that the normal velocity (N) of a wave be linearly proportional to the curvature (K) of the wavefront and that the proportionality constant be close to $\mathcal{D}_m$. In [18] we showed that these requirements are satisfied for diamond∗square combination masks; e.g., for the mask in Figure 1, $N = c - DK$ where c depends on the excitation threshold but $D \cong 3.93$ nearly independent of excitation threshold.

3. Construction of cellular automaton rules from the PDE model

Many PDE models of excitable media, when cast in dimensionless variables, take the following simple form

$$\begin{aligned} \frac{\partial \hat{u}}{\partial t} &= \epsilon \nabla^2 \hat{u} + \frac{1}{\epsilon} f(\hat{u}, \hat{v}), \\ \frac{\partial \hat{v}}{\partial t} &= \epsilon \delta \nabla^2 \hat{v} + g(\hat{u}, \hat{v}), \end{aligned} \tag{2}$$

where ϵ is a small (positive) parameter representing the ratio of time scales for changes in $\hat{u}$ (the fast variable) relative to $\hat{v}$ (the slow variable). Space has been scaled so that the diffusion coefficient of $\hat{u}$ is simply ϵ. Then δ is the ratio of diffusion coefficients of $\hat{v}$ to $\hat{u}$. The smallness of ϵ makes numerical solution of (2) difficult, but it can be exploited by singular perturbation theory [16] to show that

1. traveling wave solutions are possible for these systems;
2. away from the wavefronts and wavebacks, $\hat{u}$ changes very little, so that $f(\hat{u}, \hat{v}) \approx 0$;
3. within the wavefronts and wavebacks, $\hat{v}$ changes very little, since $\hat{v}$ is a slow variable.

It is typical of excitable media that the equation $f(\hat{u}, \hat{v}) = 0$ has three solution branches,

$$\hat{u} = h_-(\hat{v}), \qquad \hat{u} = h_0(\hat{v}), \qquad \hat{u} = h_+(\hat{v}),$$

two of which ($h_-(\hat{v})$ and $h_+(\hat{v})$) are stable. These two branches determine the value of $\hat{u}$ in the regions between wavefronts and wavebacks.

The value of $\hat{v}$ is limited by $\hat{v}_{\min} \le \hat{v} \le \hat{v}_{\max}$, where $\hat{v}_{\min}$ is the value of $\hat{v}$ at the resting state, i.e., the stable solution of $g(\hat{u}, \hat{v}) = 0$ and $f(\hat{u}, \hat{v}) = 0$. Likewise, $\hat{v}_{\max}$ is the value of $\hat{v}$ at which $h_0(\hat{v}) = h_+(\hat{v})$. At this value of $\hat{v}$, $h_+(\hat{v})$ is not stable. At $\hat{v} = \hat{v}_{\max}$, a waveback occurs as a jump from $\hat{u} = h_+(\hat{v})$ to $\hat{u} = h_-(\hat{v})$.

To convert a PDE of this sort into a cellular automaton, we introduce two new variables

$$u = \begin{cases} 0 & \textbf{if } \hat{u} = h_-(\hat{v}), \qquad \text{(recovering state)} \\ 1 & \textbf{if } \hat{u} = h_+(\hat{v}), \qquad \text{(excited state)} \end{cases}$$

and

$$v = L(\hat{v}) := \frac{\hat{v} - \hat{v}_{\min}}{\hat{v}_{\max} - \hat{v}_{\min}} v_{\text{maxaut}}.$$

In the automaton, we choose v_{maxaut} to be a large number (e.g. 1000) and convert v into an integer.

Diffusion of the variable u and the excitation jump at the wavefront are simulated by using a big mask (Figure 1) to count the number of excited cells in the neighborhood and applying a threshold function to the resulting (weighted) count, Sum. This threshold function is selected such that the correct wave speed is obtained for all values of $\hat{v}$. To construct this threshold function, first we calculate from the PDE the planar wave speed $c = c_2(\hat{v})$ of an isolated front propagating into medium with recovery value $\hat{v}$. Then, from simulations of wave propagation using the mask with threshold k, we determine the function $c_1(k)$, the planar wave speed as a function of the threshold (averaged over all directions). These two speeds should be equal (in their respective time and space scales) for all values of $\hat{v}$. Therefore

$$k(v) = c_1^{-1}\big(\alpha\, c_2\left(L^{-1}(v)\right)\big). \tag{3}$$

Here L^{-1} is an affine transformation from the automaton variable v into the PDE variable $\hat{v}$ and α transforms the units of measurement for wave speeds.

So a rule for updating u in the automaton is:

$$Sum := Mask * u^t \ ;$$

$$\textbf{if} \ \ Sum > k(v) \ \textbf{then} \ \ u^{t+1} = 1$$

$$\textbf{else} \ \ u^{t+1} = 0;$$

where the superscript refers to the time step t and '$*$' denotes convolution.

4. Time and space scales

In this section the space and time scales of the excitable medium, the PDE model, and the cellular automaton are compared. We use the units cm and s (centimeter and second) for the excitable medium, su and tu (space unit and time unit) for the PDE model and Δx and Δt for the cellular automaton.

To determine time and space scales, we use the strategy introduced by Gerhardt et al. [5,7]. The first equation to relate these scales describes the diffusion coefficient in the excitable medium (D), the PDE model (ϵ), and the cellular automaton ($\mathcal{D}_m$ as determined by (1)):

$$D\frac{cm^2}{s} = \epsilon\frac{su^2}{tu} = \mathcal{D}_m\frac{\Delta x^2}{\Delta t}. \tag{4}$$

A second relation comes from equating the speeds of a solitary plane wave (that is a plane wave propagating into resting medium):

$$V\frac{cm}{s} = c_{2\max}\frac{su}{tu} = c_1(k_{\min})\frac{\Delta x}{\Delta t} \tag{5}$$

Here, $c_{2\max} = c_2(\hat{v}_{\min})$ in the PDE is independent of ϵ as long as ϵ is small. In the CA, $k_{\min}$ is the minimum possible threshold, and $k_{\min} = k(0)$. This minimum threshold should be

large enough so that the effective diffusion coefficient is nearly independent of k for $k \geq k_{\min}$ [18].

From equations (4) and (5) one finds that the correlation between PDE and CA is

$$\begin{aligned} \Delta x &= \frac{c_1(k_{\min})}{c_{2\max}} \frac{\epsilon}{\mathcal{D}_m} su \\ \Delta t &= \left(\frac{c_1(k_{\min})}{c_{2\max}} \right)^2 \frac{\epsilon}{\mathcal{D}_m} tu, \end{aligned} \tag{6}$$

the correlation between PDE and excitable medium is

$$\begin{aligned} su &= \frac{c_{2\max}}{V} \frac{D}{\epsilon} cm \\ tu &= \left(\frac{c_{2\max}}{V} \right)^2 \frac{D}{\epsilon}\ s, \end{aligned} \tag{7}$$

and the correlation between CA and excitable medium is

$$\begin{aligned} \Delta x &= \frac{c_1(k_{\min})}{V} \frac{D}{\mathcal{D}_m} cm \\ \Delta t &= \left(\frac{c_1(k_{\min})}{V} \right)^2 \frac{D}{\mathcal{D}_m} s. \end{aligned} \tag{8}$$

We also need α, the conversion factor for wave speeds:

$$\alpha = \frac{c_1(k_{\min})(\frac{\Delta x}{\Delta t})}{c_{2\max}(\frac{su}{tu})}. \tag{9}$$

5. Update v

The update function for v is obtained directly from the PDE for $\hat{v}$:

$$\frac{\partial \hat{v}}{\partial t} = \begin{cases} g(h_+(\hat{v}), \hat{v}) & \text{if } u = 1; \\ g(h_-(\hat{v}), \hat{v}) & \text{if } u = 0; \end{cases}$$

$g(h_+(\hat{v}), \hat{v}) \geq 0$ and $g(h_-(\hat{v}), \hat{v}) \leq 0$ in the typical PDE model.

The rule for updating v in the automaton is:

if $v^t = v_{\mathrm{maxaut}}$ **then**

$$u^{t+1} = 0$$

$$v^{t+1} = v^t$$

else if $u^{t+1} = 0$ **then**

$$v^{t+1} = \max\left\{0, v^t + \lfloor L' \, g_-(v) \, \Delta t \rfloor\right\}$$

else if $u^{t+1} = 1$ **then**

$$v^{t+1} = \min\left\{v_{\mathrm{maxaut}}, v^t + \lceil L' \, g_+(v) \, \Delta t \rceil\right\},$$

where $L' = dL/d\hat{v} = v_{\mathrm{maxaut}}/(\hat{v}_{\max} - \hat{v}_{\min})$, $g_\pm = g\left(h_\pm(\hat{v}), \hat{v}\right)$ with $\hat{v} = L^{-1}(v)$, and Δt is the length of one CA time step measured in PDE time units: $\Delta t = \alpha^2 \epsilon / \mathcal{D}_m$.

If v_{maxaut} is big, the error introduced by the discretization of $\hat{v}$ (the $\lfloor \rfloor$ and $\lceil \rceil$ operations) is small.

Another rounding error is introduced by the $\min\{\cdots\}$ function. Recognizing that the jump from $u = 1$ to $u = 0$ occurs as soon as v reaches v_{maxaut}, one can determine the time of the jump within the current timestep. After the jump, v is decreased according to the rules for $u = 0$. Assuming that the increase in v, $\lceil L' \, g_+(v) \, \Delta t \rceil$ is distributed linearly over the time step, an improved rule is

if $u^{t+1} = 0$ **then**

$$v^{t+1} = \max\left\{0, v^t + \lfloor L' \, g_-(v) \, \Delta t \rfloor\right\}$$

else if $u^{t+1} = 1$ **then**

$$v_d := \lceil L' \, g_+(v) \, \Delta t \rceil;$$

if $v^t + v_d \leq v_{\mathrm{maxaut}}$ **then**

$$v^{t+1} = v^t + v_d$$

else

$$u^{t+1} = 0;$$

$$v^{t+1} = v_{\mathrm{maxaut}} + \left(1 - \frac{v_{\mathrm{maxaut}} - v^t}{v_d}\right) \lfloor L' \, g_-(\hat{v}_{\max}) \Delta t \rfloor \, .$$

If we want $\hat{v}$ to be a diffusive variable ($\delta \neq 0$ in Eq. (2)), then we complete the time step by averaging v with a square mask of an appropriate size to give the desired value of δ. Typically, we use a square mask of radius 3, so that v diffuses with $\mathcal{D}_m = 2$, i.e., $\delta = 0.5$.

Thus, a complete timestep consists of (i) application of the mask to the array of u values, (ii) the threshold function to calculate the new values for u, (iii) the rule for v (which depends on the new values of u and may change the value of u in case of $v \geq v_{\mathrm{maxaut}}$), and (iv) diffusion in v through an averaging mask.

6. Simulating the Oregonator

To complete the description of a CA model, the functions $f(\hat{u}, \hat{v})$ and $g(\hat{u}, \hat{v})$ in (1) must be specified. The Oregonator model [15] is chosen:

$$f(\hat{u}, \hat{v}) = \hat{u}(1 - \hat{u}) - \hat{f}\hat{v}\frac{\hat{u} - q}{\hat{u} + q},$$

$$g(\hat{u}, \hat{v}) = \hat{u} - \hat{v},$$

with $q = 0.002$. In all our calculations, we take $\epsilon = 0.01$.

We use $v_{\mathrm{maxaut}} = 1000$ as a compromise between roundoff error and computational complexity. For $\hat{f} = 3$ the intersection of $f(\hat{u}, \hat{v}) = 0$ and $g(\hat{u}, \hat{v}) = 0$ is $\hat{v}_{\min} = 0.00399$ and the intersection of $h_0(\hat{v})$ and $h_+(\hat{v})$ is $v_{\max} = 0.084$. The function $c_2(\hat{v})$ is calculated as the

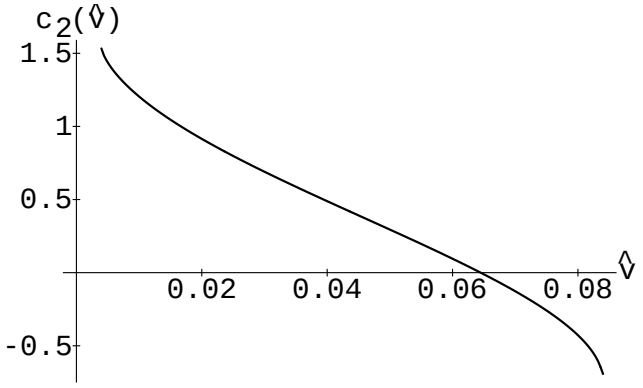

Figure 2: *Speed as a function of recovery variable $\hat{v}$ ($c_2(\hat{v})$).*

solution of the nonlinear eigenvalue problem [17]

$$x'' + c_2(\hat{v})x' + x(1-x) - \hat{f}\hat{v}\frac{x-q}{x+q} = 0,$$

$$x(-\infty) = h_-(\hat{v}), \quad x(+\infty) = h_+(\hat{v}).$$

The result for $\hat{f} = 3$ is shown in Figure 2. The speed vs. threshold function $c_1(k)$ is shown in [18], Figure 10. In order to calculate $k(v)$ (from (3)), α needs to be known. There are two possibilities: (a) fix $k_{\min}$ and calculate α from (9) or (b) fix α and calculate $k_{\min} = c_1^{-1}(\alpha c_{2\,\max})$. We use the second possibility and choose $\alpha \approx \mathcal{D}_m$, for the following reasons. The thickness of a wavefront is $\mathcal{O}(\epsilon)$ in the PDE models of excitable media [16], but it is less than one cell length in the CA model. In order that the space scale not be too small compared to the thickness of the wave front, we should require $\Delta x > \epsilon$, which implies $\alpha > \mathcal{D}_m$. However, we cannot choose α too large, because we also desire that $k_{\min} > 50$, see [18] Figure 9a. Choosing α too small does not affect u, since only the speed of wave propagation is modeled correctly for u. However, the update rules for v assume that the jumps in u at wavefronts are instantaneous, so some errors are introduced into the v dynamics if α is too small. As a compromise, in our examples, where $\mathcal{D}_m = 4$ and

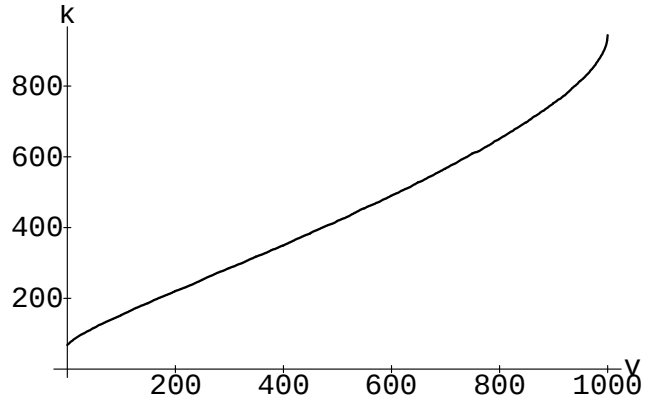

Figure 3: *Threshold as a function of automaton variable v (k(v)).*

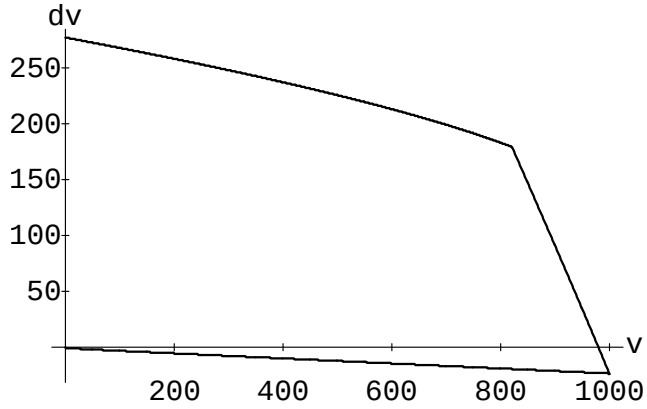

Figure 4: *Rule for v:* $v^{t+1} - v^t$ *for* $u^t = 1$ *(positive) and* $u^t = 0$ *(negative).*

$c_{2max} = 1.533$, we use $\alpha := 3$, so that $c_1(k_{\min}) = 4.599$ and $k_{\min} = 68$. The resulting function $k(v)$ is shown in Figure 3.

The updating rule for v is shown in Figure 4, where $dv = v^{t+1} - v^t$ is shown for both $u^t = 0$ and $u^t = 1$. The sharp change in dv for $u = 1$ marks the point where the jump from front to back occurs within the current time step. At $v^t \approx 1000$, the jump occurs at the beginning of the time step, therefore the behavior is essentially the same as for $u^t = 0$.

For the parameter $\hat{f}$, several values are tested. An example of a snapshot of a spiral is shown in Figure 5. Here $\hat{f} = 3$ and the diffusion coefficient for v is 2 (compared to a

diffusion coefficient of 4 for u) and therefore $\delta = 0.5$. The greylevels indicate the value of the recovery variable v. This CA simulation of the spiral wave shows many features that appear in simulations of the Oregonator PDEs by standard numerical methods [10,11].

The Oregonator is a model of the Belousov-Zhabotinskii reaction [3,15]. In this case, equations (4) and (5), which determine time and space scales, are

$$1.5 \times 10^{-5} \frac{cm^2}{s} = 0.01 \frac{su^2}{tu} = 4 \frac{\Delta x^2}{\Delta t},$$

and

$$0.013 \frac{cm}{s} = 1.53 \frac{su}{tu} = 4.59 \frac{\Delta x}{\Delta t}.$$

Thus,

$$\Delta x = 0.0075 su = 0.0013 cm,$$

$$\Delta t = 0.0225 \ tu = 0.47 s.$$

7. Comparison to the "second generation" automaton of GST

The "second generation" automaton developed by Gerhardt, Schuster and Tyson (GST) [5,6,7] was also intended to model the BZ-reaction. To compare our automaton with theirs, we reconstructed the threshold function, using a square mask of radius 6 (as in [6]). Figure 6 compares this new threshold function, for $\alpha := 4.5$, with the piecewise linear function from [6].

For updating v, GST used constant rates $v^{t+1} = v^t + g$ with $g = 20$ (when $u = 1$) and $g = -5$ (when $u = 0$). Taking into account that $v_{\mathrm{maxaut}} = 100$ in [6] and 1000 here, these values are not far from the v-updating rules in Figure 4. The major difference is that, during the recovery phase, v decreases by a constant amount in each time interval in [6],

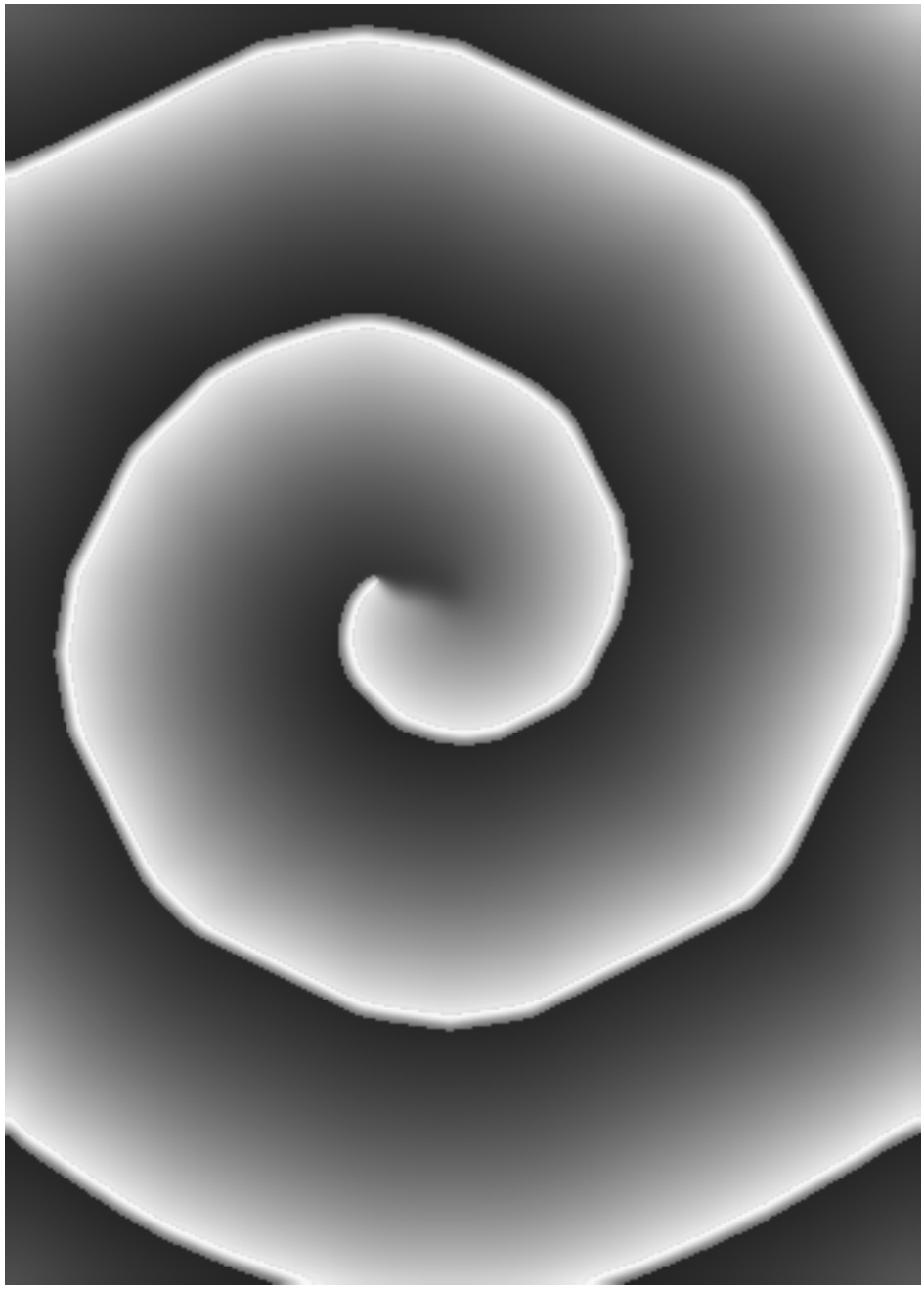

Figure 5: *Spiral wave (recovery variable v) for $\hat{f} = 3$ on a 686×960 cell domain (5.1×7.2 Oregonator space units, or 0.91×1.27 cm).*

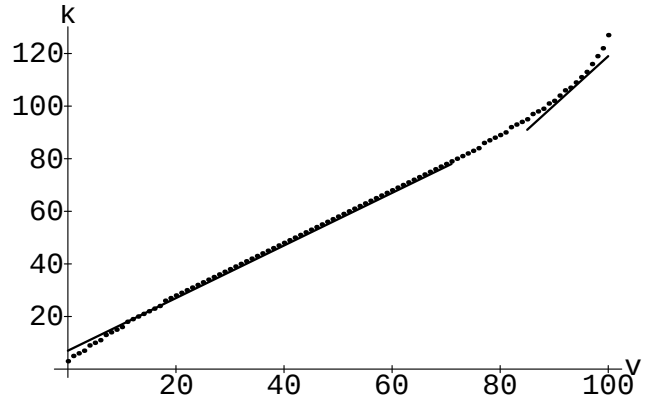

Figure 6: *Threshold $k(v)$ for the new automaton (dots) and the GST automaton (lines). In the gap from $v = 71 \cdots 85$, the GST automaton disallows changes in u.*

whereas it decreases exponentially in the model presented here. Furthermore, in [6] the values $+20$ and -5 were chosen empirically, i.e., to get a good fit of the automaton to the observed period of rotation of spiral waves in the BZ reaction. On the other hand, in our approach, the v-dynamics is derived directly from the PDE for v. A final difference is that v is nondiffusive in [6], but allowed to diffuse in the present model.

8. Comparison of cellular automaton simulations to PDE simulations

An interesting feature of solutions to the Oregonator PDEs is the meandering of the tip of a spiral for certain parameter values. A study of the meandering for different values of $\hat{f}$ and ϵ in the Oregonator model was undertaken by Jahnke and Winfree [11]. They used explicit numerical methods to solve the PDEs.

Using the automaton we study the behavior of the tip for different values of $\hat{f}$. Sections of tip traces are shown in Figure 7a. Figure 7b shows the tip traces reported in [11], using the same space scale as in Figure 7a. We observe that the tip traces from the automaton are qualitatively similar to the PDE solutions (for $\epsilon = 0.01$). The differences in spatial extent

Table 1: *Periods and wavelengths for some spirals compared to results from Jahnke and Winfree (J+W) (all in cellular automaton units).*

$\hat{f}$	λ	J+W λ_0	τ	J+W τ_0
1.4	116	144	58	70
2	147	170	65	76
3	220	228	75	90
4	245	270	87	101
6	320	354	122	124

are most likely due to differences in the method of determining the position of the tip. A different and more reliable measure of space scales is the wavelength of the spiral far from the core. Comparing wavelengths for the CA model and the PDE calculations [11] in Table 1, we see that the space scales for the two numerical approaces are nearly identical. (Note that the scaling used by Jahnke and Winfree differs by a factor of $\sqrt{\epsilon}$ in the space scale.) The time scales are also nearly the same, as witness the spiral rotation periods for CA and PDE models in Table 1. (For meandering spirals, an average over many rotations is taken.)

9. Parallel implementation

Parallel implementation on a ring-connected multicomputer is straightforward: for p processors, the simulation domain is split into p strips of equal width. Each processor stores this strip plus two overlap areas each with a width equal to the radius of the mask. At the end of each cellular automaton step, which is carried out exactly as in the sequential implementation, the information in the overlap areas is updated by messages between neighboring processors. This scheme is efficient as long as the width of each strip is larger than the size of the mask used. Some speed examples on the Intel iPSC860 hypercube with 128 processors are listed in Table 2. Here N_{int} refers to the number of cells in the x-direction assigned to each processor. In the y-direction there are 700 cells. Thus the total amount of

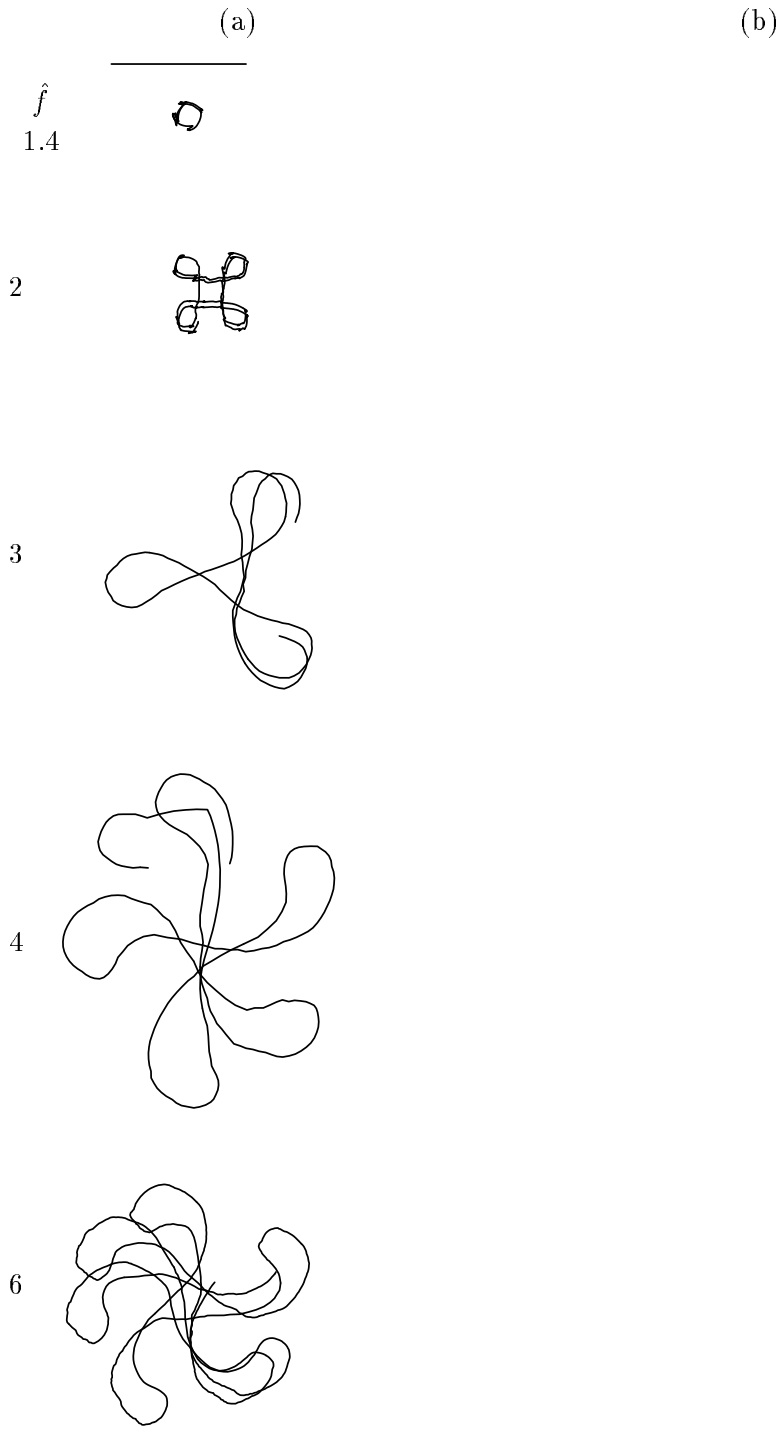

Figure 7: *Tip traces for different values of $\hat{f}$ (a) from the automaton and (b) from Jahnke and Winfree [11]. The position of the tip is the point of largest cross product of the gradients of u and v. Space scale: the length of the rule on top is 133 cells or 1 Oregonator space unit.*

Table 2: *Simulation speed on the iPSC860 hypercube. Times in μsec for one cell-update on each processor.*

processors	$N_{int} = 15$	$N_{int} = 25$	$N_{int} = 100$	$N_{int} = 400$
1	14.33	11.95	6.56	7.83
4	12.39	8.76	6.85	7.83
16	12.14	9.33	6.85	7.83
64	12.83	9.62	6.85	7.83
128	12.75	9.91	-	-

work is proportional to the number of processors. These measurements are taken without control over the load of the host processor, which is the bottleneck for small $N_{\rm int}$. Also, each reported run-time is the result of averaging 3 or 4 runs with 200 steps each. Factors influencing the performance are (i) the speed of the host and (ii) the cache hit ratio on the i860 processors. It can be seen that the overhead for higher degrees of parallelism is negligible (the execution time is independent of the number of processors if the problem size is proportional to the number of processors as in the columns of Table 2). In other words, this application belongs to the applications ideally suited even for distributed memory parallel machines.

10. Conclusion

A new way to construct a cellular automaton for simulating excitable media has been presented. The construction is based on singular perturbation analysis of the partial differential equation models for excitable media, and it shows the close relationship between the cellular automaton and the PDEs. It is not necessary to use the simulation results for tuning parameters, since all aspects of the automaton rule are derived from the PDE model. This approach is applicable to all PDE models that can be expressed in the form of (2), with a small parameter $0 < \epsilon \ll 1$. As ϵ decreases, the PDEs (2) get increasingly

difficult to solve by standard numerical methods, but the CA model gets increasingly more reliable. Indeed, we view this CA model as a non-standard numerical method for solving excitable-media PDEs when ϵ is very small (say, $\epsilon \leq 0.01$).

Since simulations of this automaton are computationally inexpensive compared to standard numerical methods for solving the PDE, three-dimensional calculations become more feasible.

References

[1] M. Courtemanche, W. Skaggs & A. T. Winfree, "Stable three-dimensional action potential circulation in the FitzHugh-Nagumo model," *Phys. D* 41 (1990), 173–182.

[2] V. G. Fast & I. G. Efimov, "Stability of vortex rotation in excitable cellular medium," *Phys. D*, (submitted).

[3] R. J. Field & R. M. Noyes, "Oscillations in chemical systems IV. Limit cycle behavior in a model of a real chemical reaction," *J. Chem. Phys.* 60 (1974), 1877–1884.

[4] R. FitzHugh, "Impulse and physiological states in models of nerve membrane," *Biophysics J.* 1 (1961), 445–466.

[5] M. Gerhardt, H. Schuster & J. J. Tyson, "A cellular automaton model of excitable media including curvature and dispersion II. Curvature, dispersion, rotating waves and meandering waves," *Phys. D* 46 (1990), 392–415.

[6] ———, "A cellular automaton model of excitable media including curvature and dispersion III. Fitting the Belousov-Zhabotinskii reaction," *Phys. D* 46 (1990), 416–425.

[7] ———, "A cellular automaton model of excitable media including curvature and dispersion," *Science* 247 (1990), 1563–1566.

[8] J. M. Greenberg, B. D. Hassard & S. P. Hastings, "Pattern formation and periodic structures in systems modeled by reaction-diffusion equations," *Bull. Am. Math. Soc.* 84 (1978), 1296–1327.

[9] J. M. Greenberg & S. P. Hastings, "Spatial patterns for discrete models of diffusion in excitable media," *SIAM J. Appl. Math.* 34 (1987), 515–523.

[10] W. Jahnke, W. E. Skaggs & A. T. Winfree, "Chemical vortex dynamics in the Belousov-Zhabotinskii reaction and in the two-variable Oregonator model," *J. of Physical Chem.* 93 (1989), 740–749.

[11] W. Jahnke & A. T. Winfree, "A survey of spiral wave behaviors in the Oregonator model," *Intern. J. of Chaos and Bifurcations* (submitted).

[12] M. Markus, "Dynamics of a cellular automaton with randomly distributed elements," in *Mathematical Population Dynamics: Proc. Second Intern. Conf.*, Marcel Dekker, New York, NY, (in press).

[13] M. Markus & B. Hess, "Isotropic cellular automaton for modeling excitable media," *Nature* 347 (Sept. 1990), 56–58.

[14] G. K. Moe, W. C. Rheinboldt & J. A. Abildskov, "A computer model of atrial fibrillation," *Am. Heart J.* 67 (1964), 200–220.

[15] J. J. Tyson, "A quantitative account of oscillations, bistability, and traveling waves in the Belousov-Zhabotinskii reaction," in *Oscillations and Traveling Waves in Chemical Systems*, R. J. Fields & M. Burger, eds., Wiley, New York, 1985, 93–144.

[16] J. J. Tyson & J. P. Keener, "Singular perturbation theory of traveling waves in excitable media (A review)," *Phys. D* 32 (1988), 327–361.

[17] J. J. Tyson & V. S. Manoranjan, "The speed of propagation of oxidizing and reducing wave fronts in the Belousov-Zhabotinskii reaction," in *Non-equilibrium dynamics in chemical systems*, C. Vidal & A. Pacault, eds., Springer-Verlag, Berlin, 1984, 89–93.

[18] J. R. Weimar, J. J. Tyson & L. T. Watson, "Diffusion and wave propagation in cellular automaton models of excitable media," *Phys. D* (previous paper).

[19] N. Wiener & A. Rosenblueth, "The mathematical formulation of the problem of conduction of impulses in a network of connected excitable elements, specifically in cardiac muscle," *Arch. Inst. Cardiol. de Mexico* 16 (1946), 205–265.

[20] A. T. Winfree, "Spiral waves of chemical activity," *Science* 175 (1972), 634–636.

[21] ———, *When time breaks down*, Princeton University Press, Princeton, NJ, 1987.

[22] A. M. Zhabotinskii & A. N. Zaikin, "Concentration wave propagation in two-dimensional liquid-phase self-oscillating system," *Nature* 225 (1970), 535–537.